JOURNAL OF THEORETICAL AND APPLIED MECHANICS
47, 4, pp. 829-853, Warsaw 2009

INVESTIGATION OF ENDWALL FLOWS AND LOSSES IN AXIAL TURBINES. PART II. THE EFFECT OF GEOMETRICAL AND FLOW PARAMETERS

Piotr Lampart

The Szewalski Institute of Fluid-Flow Machinery, Polisch Academy of Science, Gdańsk, Poland
e-mail: lampart@imp.gda.pl

Results of numerical investigations based on a 3D RANS solver FlowER, explaining the effects of geometrical and flow parameters on the development of endwall flows are presented. The blade height-to-chord ratio, flow turning in the cascade, inlet angle and radial distribution of pressure and profile load are considered here. It is also shown how the secondary flow patterns change in the case of non-nominal incidence at the suction side of the blade and due to interaction with shroud leakage and periodical turbine wakes.

Key words: axial turbine, endwall flow, secondary flow, enthalpy loss

1. Introduction

As shown in part I of this paper (Lampart, 2009), endwall losses in turbine cascades at some spanwise positions per unit length can exceed the profile losses by several times. Secondary loss centres are usually located some way from the mid-span section. For turbine cascades of low aspect ratios and high flow turning, the loss contours originating from the opposite endwalls can interfere at mid-span sections to form a strong single loss centre. The contribution of the secondary losses in the total loss balance is increased then.

In this part of the paper, the development of secondary flows in axial turbines is investigated with the help of CFD, using the code FlowER, Yershov and Rusanov (1997), Yershov *et al.* (1998). The investigations are carried out using stator and rotor cascades of HP turbines. The calculations of the effect of relative blade height and flow turning are made in a certain range of blade height, number of stator/rotor blades, mid-span diameter, profile chord, cascade pitch, stagger angles and inflow angles. Besides, the effect of spanwise

distribution of pressure and profile load as well as the effect of shroud leakage and periodical wakes on the secondary flow losses are investigated. Secondary flow patterns in the case of non-nominal incidence at the suction side of the blade are also explained.

2. The effect of relative blade height

In this Section it is shown how the development of secondary flows and endwall losses is affected by the blade height for two investigated types of profiles – rear-loaded stator profile PŁK [11] and impulse rotor profile R2, Dejch *et al.* (1965). The calculations were made for three blade heights – $h = 20\,\text{mm}$, $60\,\text{mm}$ and $100\,\text{mm}$, while keeping the other geometrical parameters of the cascades unchanged, that is mid-span diameter – $D = 872\,\text{mm}$, profile chord $75\,\text{mm}$ (stator) and $35\,\text{mm}$ (rotor), blade number $z = 50$ (stator) and 118 (rotor), stagger angle $\beta_u = -44°$ (stator) and 14° (rotor), assuming the nominal inlet angles. The aspect ratio (blade height-to-chord ratio) changes then in the range $h/c = (0.27\text{-}1.33)$ (stator) and (0.56-2.78) (rotor). The assumed pressure drop ratio in the stage is typical for low-load HP turbine stages – $p_{ex}/p_{in} = 0.9$ (pressure decrease from 79.1 to 71.2 bar). For this load, the exit Mach number is equal to 0.4 (stator) and 0.3 (rotor).

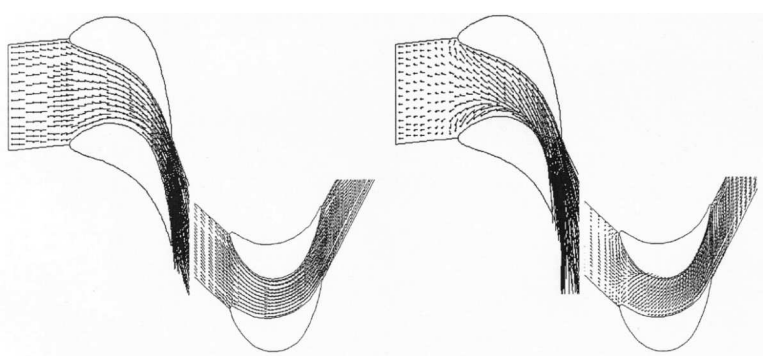

Fig. 1. Velocity vectors at the mid-span section (left) and at the root (right) in the stator (left) and rotor (right) cascades; blade height $h = 60\,\text{mm}$

The comparison of velocity vectors at the mid-span section and at the root of the stator and rotor cascade is presented in Fig. 1 (for the medium-height blades). The process of expansion is regular at the mid-span, whereas an endwall crossflow is observed at the root. The picture of velocity vectors

looks different in the case of the stator and rotor cascade, which is connected with the distribution of load in both cascades. In the case of the considered impulse rotor profile, the pressure difference between the pressure and suction surface exceeds the inlet-to-exit pressure difference just downstream of the leading edge. In the aft-loaded stator cascade, the pressure-to-suction side pressure difference becomes close to the inlet-to-exit pressure difference at the mid-chord section, which can be observed in Fig. 2. Therefore, in the case of rotor cascade, fluid elements from the endwall boundary layer are transported, under the effect of crossflow pressure gradient, onto the suction surface nearer to the leading edge as compared to the stator cascade. This gives a rise to the intensification of secondary flows in the case of the rotor cascade.

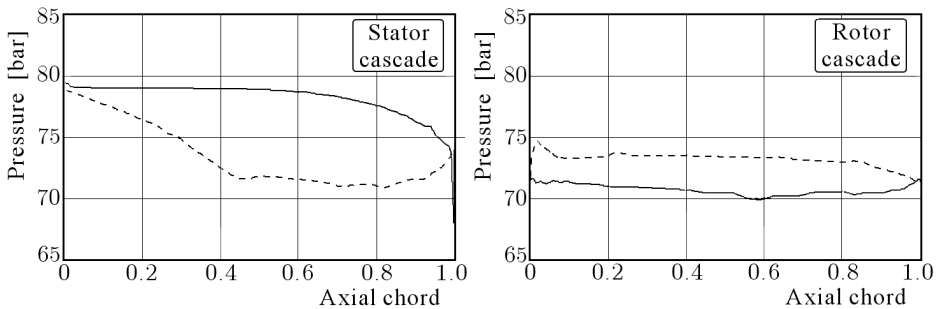

Fig. 2. Pressure distribution at the stator (left) and rotor (right) profile; blade height $h = 60\,\text{mm}$

The comparison of velocity vectors at the suction side of the stator and rotor blades for two values of blade height $h = 20\,\text{mm}$ and $100\,\text{mm}$ is illustrated in Fig. 3, from which the spanwise extension of the secondary flow regions in respective cascades can be estimated. For the same blade height, this extension is larger for the rotor cascade. For long blades, the secondary flows develop only near the endwalls, whereas for short blades, the secondary flows reach the mid-span section, which is especially clear for the rotor cascade.

Entropy function ($\sigma = p/\rho^{\kappa}$) contours in radial sections subsequently located downstream of the leading edge in the stator and rotor cascades for three values of blade height $h = 20\,\text{mm}$, $60\,\text{mm}$ and $100\,\text{mm}$ are presented in Figs. 4 and 5. The sections are made in the blade-to-blade region, at the trailing edge and downstream of it, illustrating the successive increase of entropy and formation of loss centres for different profile types and blade heights. Within the blade-to-blade region, the process of building of the passage vortex is observed. For cascades of blade height $h = 60\,\text{mm}$ and $100\,\text{mm}$, the region of profile losses and two local centres of secondary losses can be distinguished.

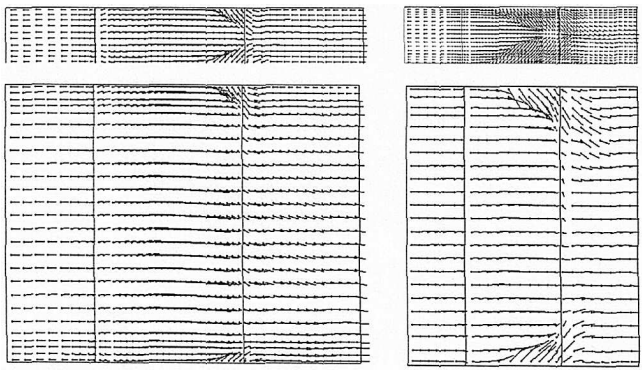

Fig. 3. Velocity vectors at the suction surface in the stator (left) and rotor (right) cascade for the blade height of $h = 20\,\text{mm}$ (top) and $100\,\text{mm}$ (bottom)

Downstream of the trailing edge, the extension of the secondary flow region in the stator cascade slightly exceeds the width of the 2D wake, whereas in the rotor cascade, the secondary flow region occupies a considerable part of the flow channel. For cascades of blade height $h = 20\,\text{mm}$, the profile losses and secondary flow losses originating from both endwalls merge to form a large loss centre at the midspan. A conspicuous difference between the stator and rotor cascade for the blade height of $h = 20\,\text{mm}$, which can be observed from Figs. 4 and 5, is that in the latter case the passage vortices merge at the midspan already upstream of the trailing edge, whereas for the stator cascade they meet only downstream of the trailing edge.

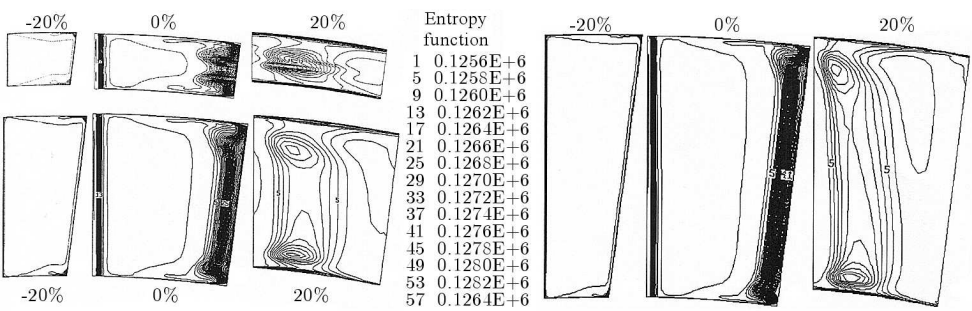

Fig. 4. Entropy function contours in three subsequent radial sections of the stator cascade of blade height $h = 20\,\text{mm}$ (top left), $60\,\text{mm}$ (bottom left) and $100\,\text{mm}$ (right); the numbers indicate location of a section downstream of the leading edge as per cent of the axial chord

The observed phenomena have an effect on the spanwise distribution of enthalpy losses (referred to the isentropic enthalpy drop in the cascade) and

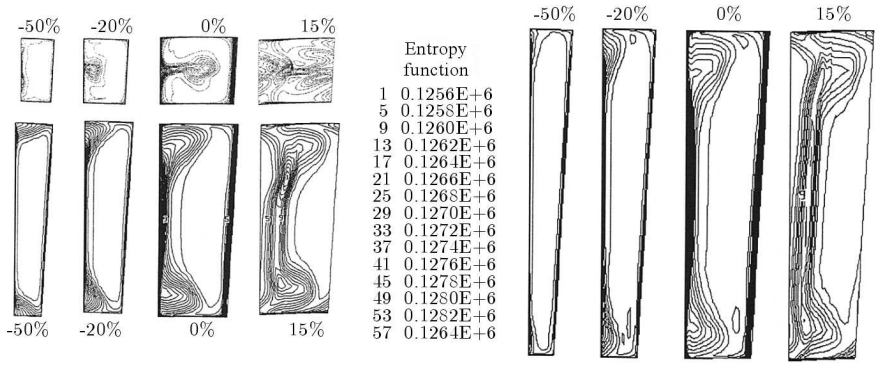

Fig. 5. Entropy function contours in three subsequent radial sections of the rotor cascade of blade height $h = 20\,\text{mm}$ (top left), $60\,\text{mm}$ (bottom left) and $100\,\text{mm}$ (right); the numbers indicate location of a section downstream of the leading edge as per cent of the axial chord

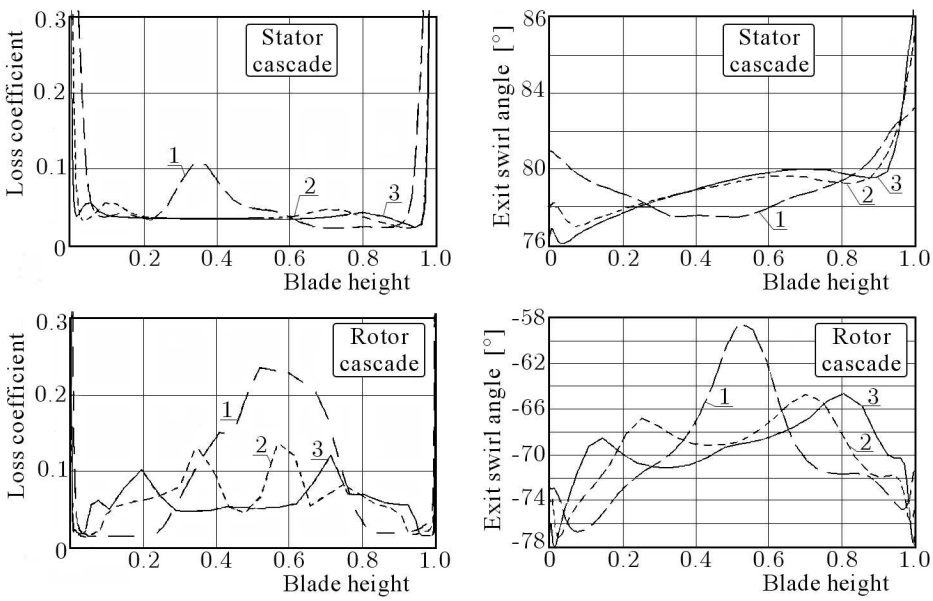

Fig. 6. Spanwise distribution of enthalpy losses (left) and exit angle (right) in the stator (top) and rotor (bottom); 1 – $h = 20\,\text{mm}$; 2 – $h = 60\,\text{mm}$, 3 – $h = 100\,\text{mm}$

exit angle presented in Fig. 6. With the decreasing blade height, the flow losses are increased due to the increased contribution of secondary flow losses. Also the secondary loss centres are located further away from the endwalls. Below a certain crtical value of the aspect ratio, one secondary flow loss centre near the mid-span is observed and the profile loss can not be estimated from the

picture. Secondary flows also change the distribution of exit or turning angle in the cascade[1]. In the secondary flow region, there is an underturning on the side of the mid-span and overturning on the side of the endwalls. For the investigated cascades of blade height of $h = 60\,\mathrm{mm}$ and $100\,\mathrm{mm}$, changes of the exit flow angle in the region of secondary flows, with respect to the main annular flow away from the endwalls, do not exceed 2° in the case of the stator cascade and 4° in the rotor cascade. The changes are much larger for cascades of blade height $h = 20\,\mathrm{mm}$ and exceed 10°, see also Gardzilewicz *et al.* (2000).

3. The effect of flow turning in the cascade

An important factor in the development of secondary flows is the flow turning in the cascade. Besides the profile shape, the level of flow turning is controlled by the profile stagger angle, cascade density and inlet angle.

First, we investigate the effect of flow turning on the development of secondary flows by changing the inlet angle (still within the near-nominal region of operation). Particularly sensitive to the inlet flow angle are rotor cascades of impulse turbine stages. The results of investigations presented in Figs. 7-10 concern the rotor cascade with profiles of type R2 for blade height $h = 60\,\mathrm{mm}$, for three inlet angles $\alpha_0 = 55^\circ, 63^\circ, 70^\circ$. It follows from the picture of static pressure in the blade-to-blade passage (Fig. 7) that the increase of the inlet angle moves the stagnation point towards the pressure side of the blade, which in turn leads to an increase of the pressure-to-suction side pressure difference and intensification of crossflow in the endwall boundary layer from the concave to convex surface of the neighbouring blades. This can be observed from velocity vectors at the endwall presented in Fig. 8. As a result, an increase of the inlet angle and at the same time increase of the flow turning in the cascade (the mean value of the exit angle practically remains unchanged and is equal to -69°) leads to an increase in the circulation and size of passage vortices. The passage vortex centres move towards the mid-span section, as can be seen from Fig. 9, showing the secondary flow vectors at the trailing edge and total pressure contours in a section located 15% of the axial chord downstream of the trailing edge. An increase of profile losses and mixing losses in the region of secondary flows takes place. The non-uniformity in the distribution of the

[1]It is understood that the rotor cascade lies in the wake of the stator cascade, so the rotor profile is reflected with respect to the axis normal to the cascade front with the corresponding change of sign of the inlet and exit angles.

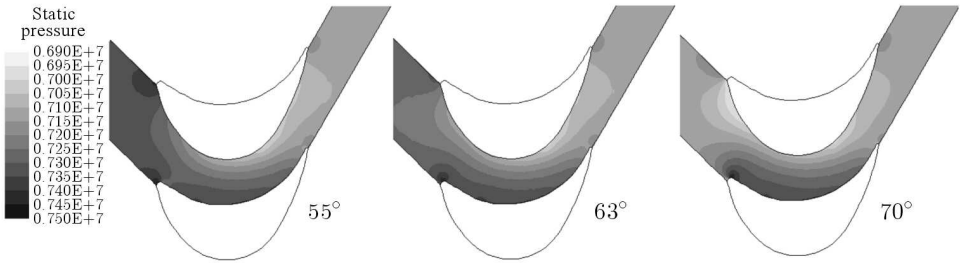

Fig. 7. Static pressure contours at the mid-span of the rotor cascade for three inlet angles $\alpha_0 = 55°, 63°, 70°$

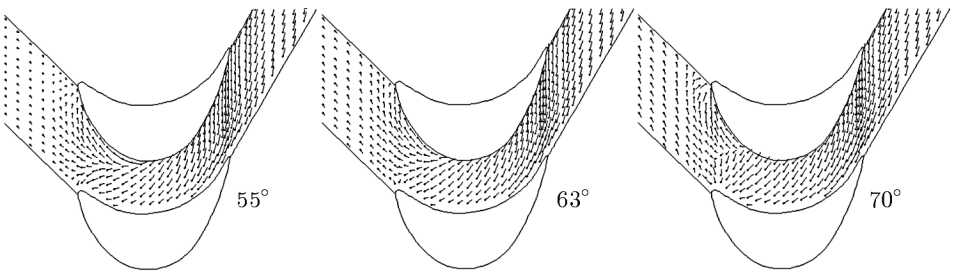

Fig. 8. Velocity vectors at the endwalls of the rotor cascade for three inlet angles $\alpha_0 = 55°, 63°, 70°$

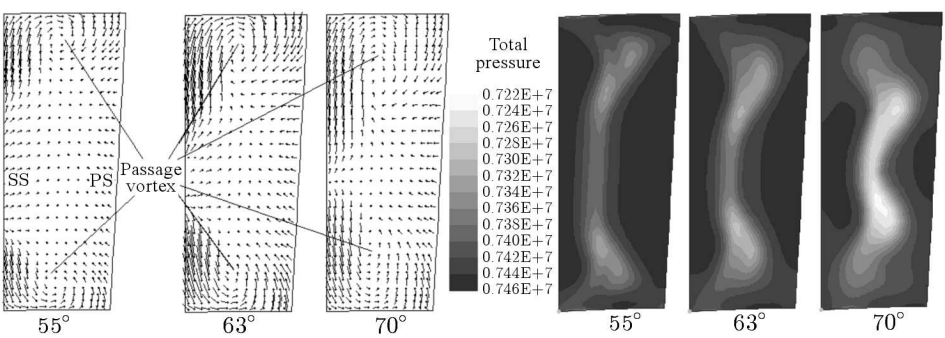

Fig. 9. Secondary flow vectors at the trailing edge and total pressure contours 15% axial chord downstream of the trailing edge in the rotor cascade for three inlet angles $\alpha_0 = 55°, 63°, 70°$ (PS – pressure surface, SS – suction surface)

exit angle is also increased, whereas the mean value of the exit angle remains unchanged, Fig. 10. Although the assumed range of variation of the inlet angle is relatively narrow, changes in the flow patterns and the resulting loss characteristics are considerable and very clear in the presented pictures.

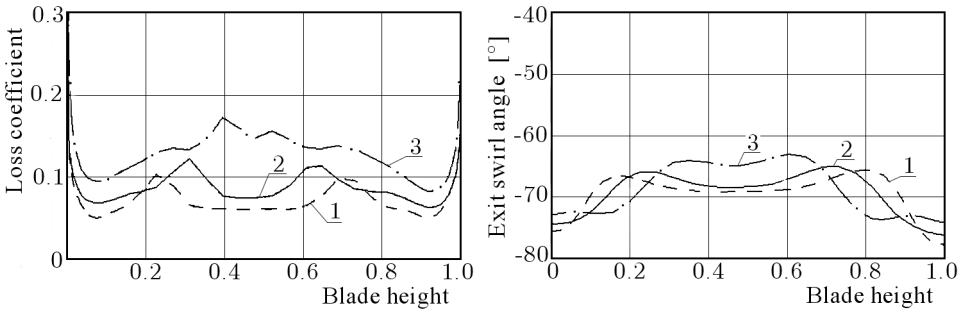

Fig. 10. Spanwise distribution of enthalpy losses (left) and exit angle (right) in the rotor 45% axial chord downstream of the trailing edge; 1 – $\alpha_0 = 55°$, 2 – $\alpha_0 = 63°$, 3 – $\alpha_0 = 70°$ ($\alpha_{1av} = -69°$)

It is also interesting to observe the effect of flow turning on the development of secondary flow and tip leakage as well as on the interaction of the two flows in a cascade with a tip clearance. In Fig. 11, showing secondary flow vectors and total pressure contours in subsequent sections upstream and downstream of the cascade trailing edge, the case of a relatively lower flow turning and lower load of an investigated HP cascade is presented (profile stagger angle $-13°$, inlet angle $63°$, exit angle $-63°$, Ma = 0.2). In this case, a quick disintegration of the tip passage vortex is observed as a result of interaction with a more intensive structure of the tip leakage vortex and the moving endwall in Fig. 11. The passage vortex can be distinguished as a counter-rotating structure within the blade-to-blade passage, but it is already dissipated at the trailing edge.

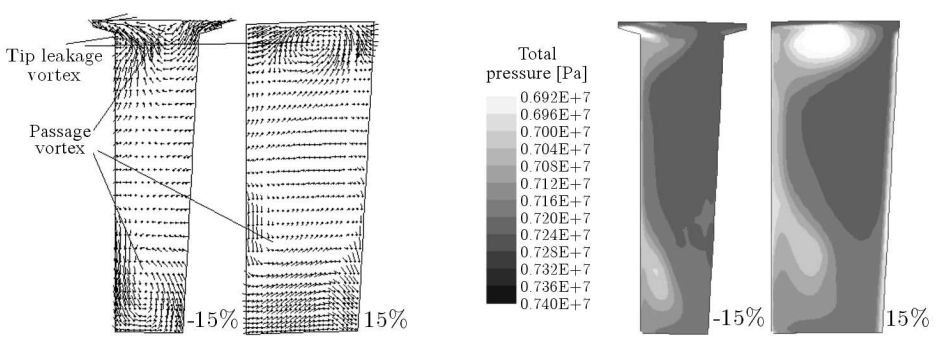

Fig. 11. Secondary flow vectors and total pressure contours in the HP rotor cascade in selected sections located 15% axial chord upstream of the trailing edge, at the trailing edge and 15% axial chord downstream of it; tip gap size – 2%, Ma = 0.2, $\alpha_0 = 63°$, $\alpha_1 = -63°$

The interaction of the tip leakage vortex and passage vortex looks quite different in the case of a larger flow turning and larger load of the cascade (profile stagger angle $-18°$, inlet angle $75°$, exit angle $-72°$, Ma $= 0.4$) illustrated in Fig. 12. In this case, the role of the cross-flow in the endwall region is increased. The passage vortex is formed long before the tip leakage vortex. The tip leakage pushes the passage vortex towards mid-span sections, rolls up into a tip leakage vortex blocking further cross-flow that is formed near the trailing edge. This cross-flow can possibly be rolled up again at the pressure surface above the tip leakage vortex. If this happens, the new passage vortex is quickly dissipated by the interaction with the stronger tip leakage vortex.

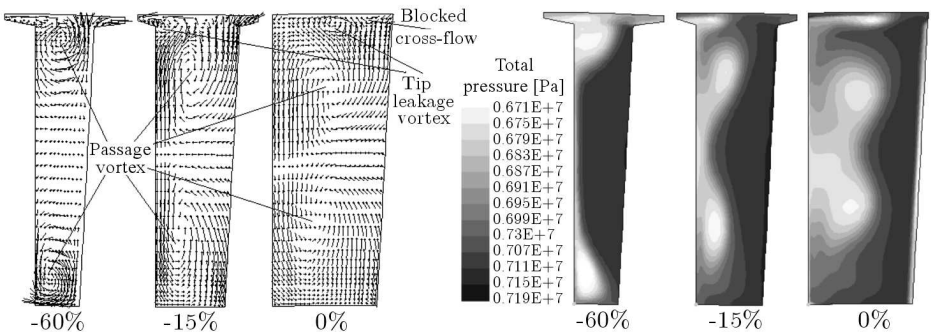

Fig. 12. Secondary flow vectors and total pressure contours in the HP rotor cascade in selected sections located 60% and 15% axial chord upstream of the trailing edge and at the trailing edge; tip gap size – 2%, Ma $= 0.4$, $\alpha_0 = 75°$, $\alpha_1 = -72°$

The increased flow turning in the cascade usually means increased secondary flow losses, see also Traupel (1977). However, high turning profiles are used to increase the blade load and produced power as well as increase the turbine power-to-weight ratio. Thus, it is important to consider also highly-loaded blading systems such as those of Yamamoto *et al.* (2001), where the flow turning is equal to about $160°$ (with the design inlet and exit angles of about $\pm 80°$). This model air cascade is also investigated in the present paper to find out the effect of secondary flows on its performance. Nominal flow conditions are assumed (chord and exit velocity based Reynolds number $\mathrm{Re} = 1.4 \cdot 10^5$, inlet overpressure $p_{Tin} = 1.025$). The computations include the leakage flow over unshrouded blades.

Velocity vectors coloured by Mach numbers at hub, mid-span and tip sections of the investigated highly-loaded rotor cascade are illustrated in Fig. 13.

An intensive hub endwall crossflow reaches the suction surface just at the front part of the blade. At the tip, the division of the tip leakage and secondary flow streams takes place near/over the pressure surface of the blade tip.

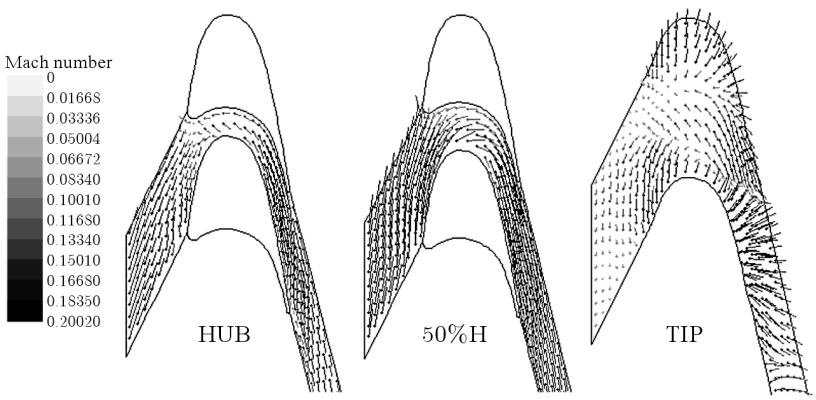

Fig. 13. Velocity vectors in subsequent sections from hub to tip

Total pressure contours in subsequent sections located 40% and 70% of the axial chord downstream of the leading edge, at the trailing edge and also 25% of the axial chord downstream of the trailing edge are illustrated in Fig. 14. The passage vortices are already developed and meet at the mid-span well upstream of the trailing edge. The interaction of the passage vortex tends to push the developed upper passage vortex towards the pressure surface of the blade. The obtained computational flow patterns downstream of the trailing edge are similar to those observed experimentally by Yamamoto *et al.* (2001) (Fig. 15), showing a strong skewed loss center due to the interaction of passage vortices at the mid span and a large region occupied by the tip leakage vortex.

A span-wise distribution of enthalpy losses in the Yamamoto cascade in a section located 30% of the axial chord downstream of the trailing edge is presented in Fig. 16. Secondary flow and tip leakage losses are very high in this cascade. It is difficult to evaluate particular loss components and distinguish the profile losses. The lower passage vortex washes away and entrains the profile boundary layer from the suction surface. Therefore, the loss distribution shows reduced values at the lower part of the channel, shifting the loss core towards the mid-span. The calculated mass averaged cascade loss at this section is equal to 23.7%, the mixed-out value of loss exceeds 30%.

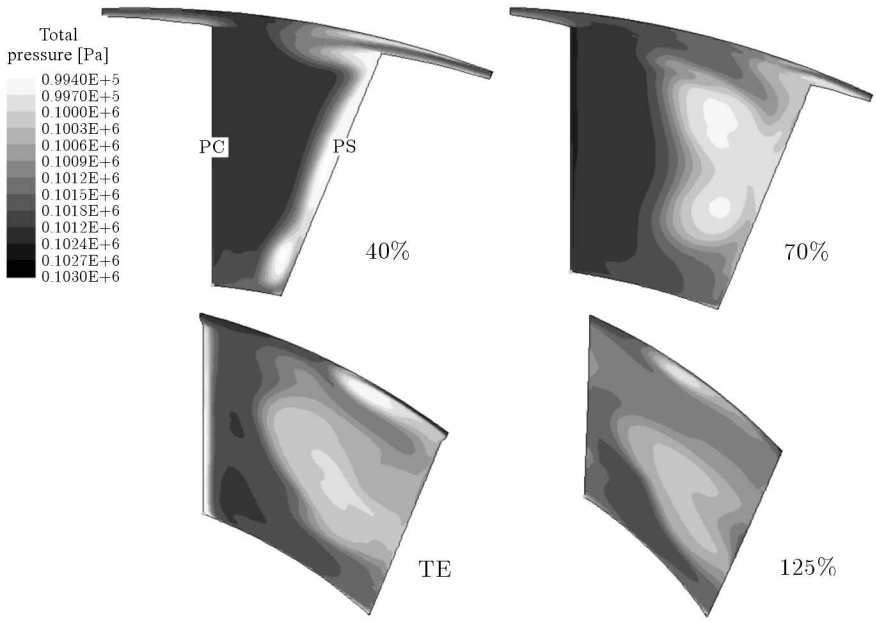

Fig. 14. Total pressure contours in subsequent radial sections from the inlet to exit of the Yamamoto cascade. The numbers denote location of sections with respect to the leading edge as per cent of the axial chord; TE – trailing edge

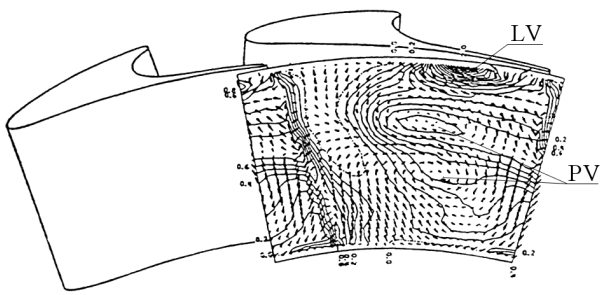

Fig. 15. Secondary flow vectors and loss contours upstream (left) and downstream (right) of the trailing edge – measurement results from Yamamoto *et al.* (2001)

4. The case of non-nominal inflow onto the suction side of the blade

Typically, a high non-nominal incidence angle at the cascade means the presence of a separation zone which decreases the flow efficiency. The separation zone occurs at the pressure side, while the inflow is moved onto the suction

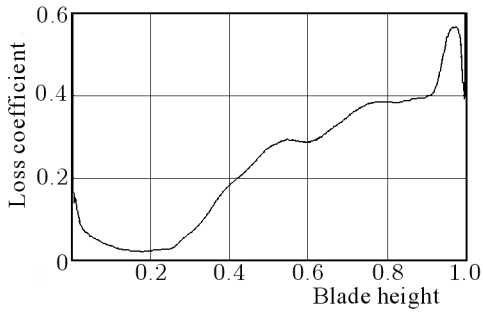

Fig. 16. Span-wise distribution of losses in the Yamamoto cascade

side and the reverse. The non-nominal incidence affects also the development of secondary flows. Particularly unusual is the formation of secondary flows under conditions of non-nominal incidence moved onto the suction side of the blade.

Situations of non-nominal incidence discussed in this Section usually take place when the blading system operates under variable load conditions. Locally, the non-nominal incidence onto the suction surface is a typical phenomenon in the region of influence of side flows, especially leakage flows over/under shrouded/unshrouded rotor/stator blades.

Detailed investigations of the effect of non-nominal incidence onto the suction surface on the development of secondary flows are conducted for the HP rotor cascade (of type R2) for $\alpha_0 \in \langle 0°, 30° \rangle$. A key factor in the development of secondary flows is the distribution of static pressure within the channel. Static pressure contours and velocity vectors at the endwall of the investigated cascade for the case of non-nominal inflow onto the suction side of the blade are presented in Fig. 17. The stagnation point is observed to move considerably along the suction surface by up to 10% of the axial chord. In the front part of the flow channel, the role of the convex and concave surfaces is practically reversed. The former assumes the role of the pressure surface, whereas the latter becomes the suction surface. A return to the situation typical for the turbine channel flows takes place in the middle part of the channel. This distribution of pressure modifies the picture of crossflows in the endwall boundary layer and the pattern of secondary flows. Under these conditions, two types of endwall crossflow are observed. A dominant crossflow in the endwall boundary layer, especially in the first part of the channel is the reverse crossflow from the convex to concave surface, which is opposite to the regular endwall crossflow at nominal incidencies. Another crossflow from the concave to convex surface (regular crossflow) is also observed further downstream in

the central and rear part of the channel. Both crossflows are blocked roughly in the middle of the blade-to-blade distance and roll up into vortices.

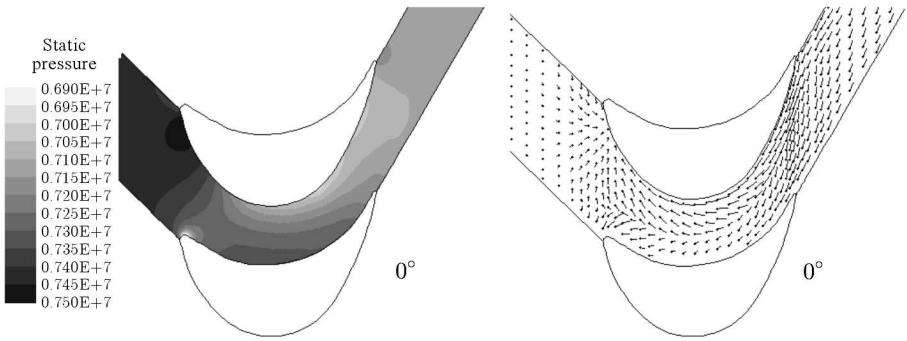

Fig. 17. Static pressure contours and velocity vectors at the endwall of the rotor cascade for the case of non-nominal inflow onto the suction side of the blade, $\alpha_0 = 0°$

The development of secondary flows for the case of non-nominal inflow onto the suction side of the rotor blade for incidence angles of $\alpha_0 = 0°$ and $30°$ can be observed in Fig. 18 showing secondary flow vectors in subsequent sections upstream of the trailing edge of the rotor cascade. First to appear is the reverse passage vortex originating from the reverse crossflow from the stagnation point moved onto the convex surface, which is blocked in the middle of the blade-to-blade passage and rolled up. One can also expect that the suction side of the horse-shoe vortex will also be rolled up into this vortex. Further downstream, another vortex structure is observed originating from the regular crossflow from the concave to convex surface – a passage vortex. For the incidence of $\alpha_0 = 30°$, the reverse passage vortex is quickly dissipated so that only the passage vortex is present at the trailing edge section. The regular endwall crossflow reaches the opposite blade surface (suction surface) in the rear part of the channel, therefore the passage vortex finally develops at the suction surface of the blade. For the incidence of $\alpha_0 = 0°$, both vortex structures – the passage vortex and reverse passage vortex are well preserved. The weaker passage vortex remains located at the pressure surface and is pushed towards the mid-span, whereas the stronger reverse passage vortex occupies the central part of the flow channel. A change of sign of the inlet angle and reduction of flow turning with a further inflow onto the suction surface leads to an increase of circulation and size of the reverse passage vortex.

In the investigated cases of non-nominal inflow onto the suction surface of the blade, the total pressure contours have a different shape than in the case of nominal inflow, which can be seen in Fig. 19 showing the distribution

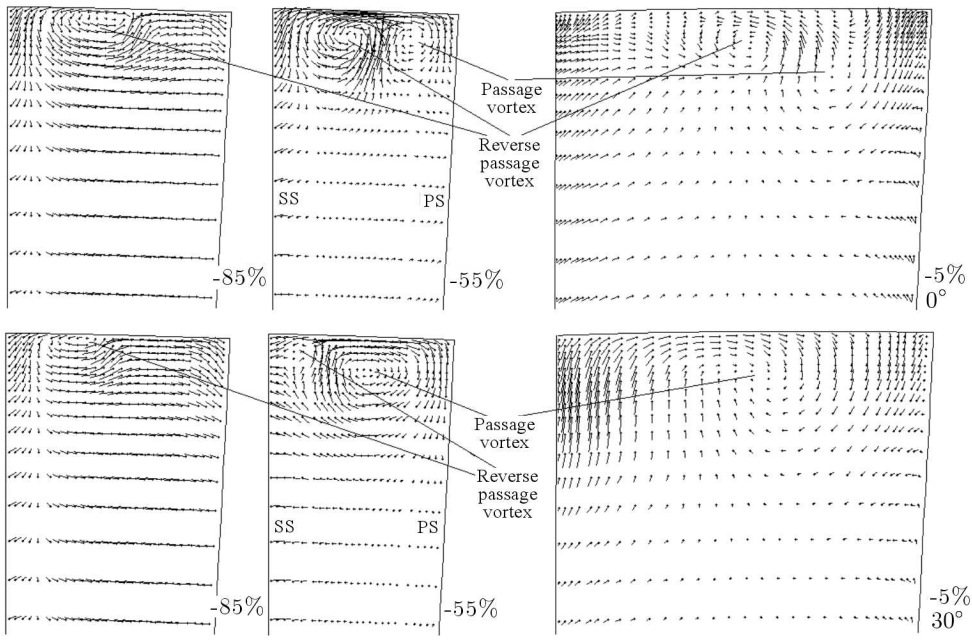

Fig. 18. Secondary flow vectors 85%, 55% and 5% axial chord upstream of the trailing edge of the rotor cascade for the case of non-nominal inflow onto the suction side of the blade for $\alpha_0 = 0°$ (top) and $30°$ (bottom); SS – suction (convex) surface, PS – pressure (concave) surface

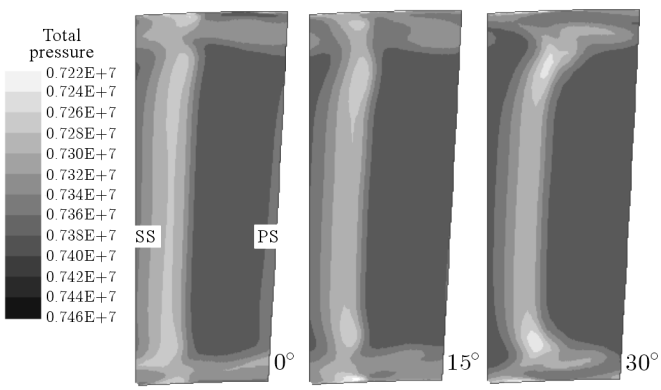

Fig. 19. Total pressure contours 15% axial chord downstream of the trailing edge of the rotor cascade for the case of non-nominal inflow onto the suction side of the blade for $\alpha_0 = 0°$, $15°$, $30°$; SS – suction (convex) surface, PS – pressure (concave) surface

of the total pressure in a section located 15% of the axial chord downstream of the trailing edge for three angles of incidence $\alpha_0 = 0°$, 15°, 30°. With the decreasing inlet angle, the wake becomes more and more straight but is thicker. A considerable increase in the level of profile losses is observed. The losses due to the passage vortex decrease and concentrate nearer to the wake axis. The losses that concentrate at a short distance from the endwall outside of the wake axis are due to dissipation of the reverse passage vortex. The spanwise distribution of enthalpy losses and exit angle downstream of the rotor trailing edge for three angles of incidence $\alpha_0 = 0°$, 15°, 30° is depicted in Fig. 20. This picture confirms the increasing profile and endwall losses with the decreasing inlet angle (moving the incidence towards the suction surface). On the other hand, the level of non-uniformity of the exit flow angle near the endwall is decreased. More information on the effects of non-nominal incidence flows can be found in Lampart (2006a).

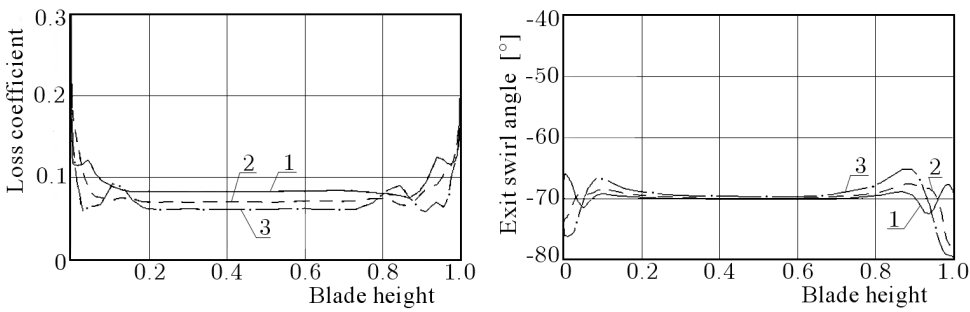

Fig. 20. Spanwise distribution of enthalpy losses (top) and exit angle (bottom) 45% axial chord downstream of the trailing edge; 1 – $\alpha_0 = 0°$, 2 – $\alpha_0 = 15°$, 3 – $\alpha_0 = 30°$ ($\alpha_{1av} = -69°$)

5. The effect of span-wise distribution of static pressure and cascade load

The span-wise distribution of static pressure and cascade load are other parameters that have an effect on the development of secondary flows and losses. These parameters are important for 3D-shaped blades, however it should also be remarked that the spanwise distribution of static pressure in flow turning annular cascades of straight blades is yet not uniform – typically a hub-to-tip pressure increase is observed in stationary cascades. This leads to migration of

low kinetic energy fluid elements from boundary layers on the profile (especially in the rear part where the boundary layer is the thickest), wakes and other vortical structures towards the hub. In typical stationary annular cascades, endwall losses tend to be higher at the hub rather than at the tip endwall. On the other hand, in rotating annular cascades, usually migration of low kinetic energy fluid elements towards the tip is observed due to the action of centrifugal forces. The development of secondary flows is also affected by their interaction with leakage flows.

Basic concepts of 3D turbine blading were presented by Denton and Xu (1999). In the paper of Lampart and Gardzilewicz (1999), effects of several methods of 3D blade shaping on flow in a low-load impulse HP turbine stage with PŁK and R2 profiles are described. Let us consider the case of stator blade compound lean, illustrated in Fig. 21, where the stator blade profiles at the hub and tip are non-linearly displaced in the circumferential direction with respect to the mid-span profile, increasing the displacement towards the endwalls. The pressure surface of the compound leaned blade forms an acute angle with the endwalls. The investigations were conducted for the blade apsect ratio of 0.75 (stator), 1.3 (rotor), pressure drop in the stage from 79.08 to 71.16 bar, stator exit Mach number of $\mathrm{Ma} = 0.4$.

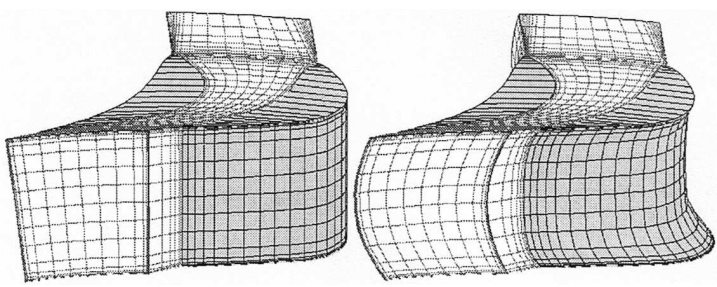

Fig. 21. Straight and compound leaned stator blade

There is a considerable redistribution of flow parameters between the stage with straight and compound leaned stator blades, which can be observed in Fig. 22, showing spanwise distributions of the pressure, relative velocity and swirl angle close to the cascade trailing edges. It refers both to the region of the modified stator and the rotor whose geometry was not modified. An increase of the static pressure at the endwalls in the compound leaned stator leads, first, to a decrease of the flow velocity there and a reduction of endwall boundary layer losses, second, to a transport of the endwall and profile boundary layer fluid towards the mid-span due to a spanwise pressure gradient towards the mid-span. The intensity of the passage vortices is decreased, the thickness

of the wake at the mid-span is increased. The above described tendency can be viewed from Fig. 23 showing the comparison of entropy function contours downstream of the cascade trailing edges for the original and modified blading system. In the compound leaned stator blades, the weight of flow losses in the stator is shifted towards the mid-span and the level of losses is decreased near the endwalls, which can be seen from the spanwise distribution of losses illustrated in Fig. 25. The flow turning increases at the midspan and decreases at the endwall as compared to the original blade, Fig. 22.

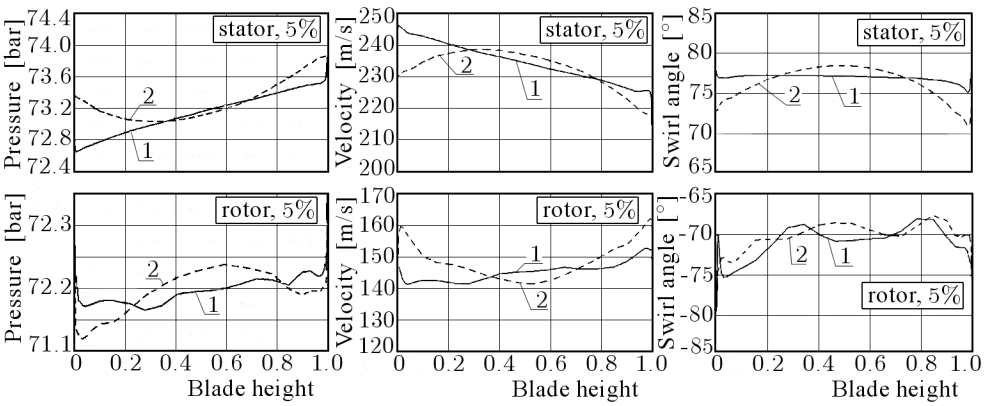

Fig. 22. Spanwise distribution of static pressure (left), relative velocity (centre) and swirl angle (right) in the stator (top) and rotor (bottom) 5% axial chord upstream of the trailing edge; stage with straight stator blades (1), stage with compound leaned stator blades (2)

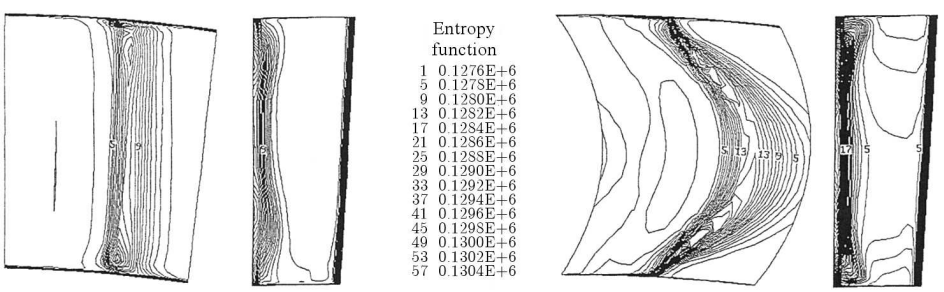

Fig. 23. Entropy function contours in the stator (10% axial chord downstream of the trailing edge) and rotor (at the trailing edge); stage with straight stator blades (left of key), stage with compound leaned stator blades (right of key)

The spanwise redistribution of static pressure at the exit from the stator leads to a spanwise redistribution of load in the rotor cascade. For the case of stator blade compund lean, there is a velocity increase at the rotor endwall,

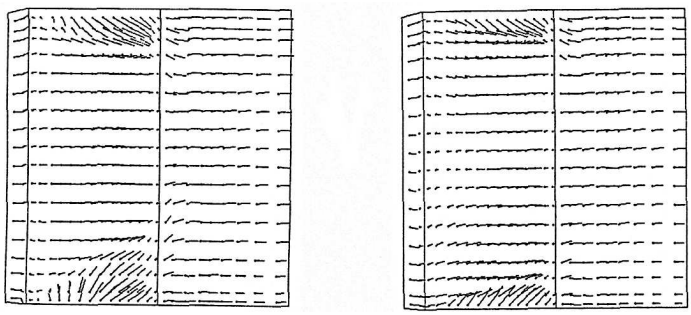

Fig. 24. Velocity vectors at the suction side of the rotor blade; the stage with straight stator blades (left), the stage with compound leaned stator blades (right)

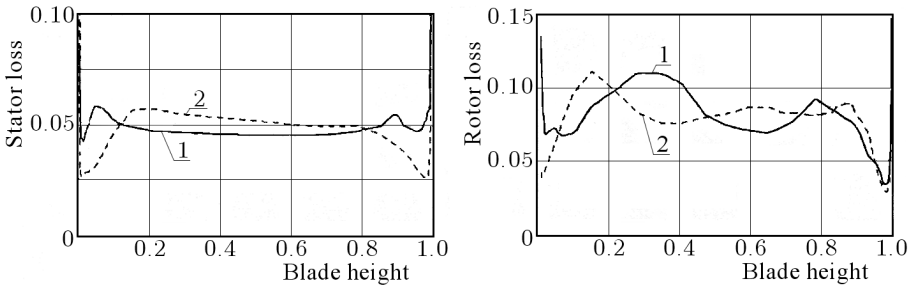

Fig. 25. Span-wise distribution of enthalpy losses in the stator (left) and rotor (right); the stage with straight stator blades (1), the stage with compound leaned stator blades (2)

Fig. 22, which can lead to an increase of the boundary endwall losses. However, a spanwise extension of the secondary flow zones in the rotor is reduced in Fig. 24, showing velocity vectors at the suction surface of the rotor blades. The secondary loss centres remain closer to the endwalls as illustrated by the entropy function contours at the exit section, Fig. 24, and by the spanwise distribution of enthalpy losses in the rotor, Fig. 25. A redistribution of the rotor exit swirl angle is also observed, Fig. 22. The summary effect in the form of efficiency rise or loss depends on the original geometry, applied shape modification and operational parameters of the turbine stage.

6. The effect of leakage flow (the case of shrouded blades)

Leakage flows have an effect on the development of secondary flows in a blade row where the leakage is originated as well as in the subsequent blade row. The interaction of leakage flows with the main stream and secondary flows

is investigated numerically using the flow solver FlowER with source/sink-type boundary conditions, which are used at places at the endwalls referring to the designed locations of injection of hub and tip leakage flows into, or their extraction from the blade-to-blade passage, see Fig. 26. The method is described in more detail by Lampart *et al.* (2004).

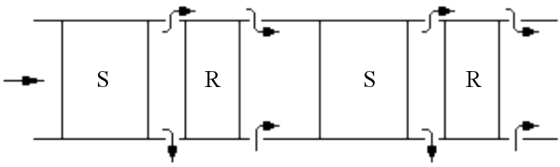

Fig. 26. Computational domain with source/sink-type permeable boundaries to simulate the effect of hub and tip leakage flows in impulse turbines; S – stator, R – rotor

The flow in a group of two HP impulse stages (coming from a 200 MW steam turbine) with short-height straight blades with PŁK (stators) and R2 (rotors) profiles was investigated. The characteristic blade dimensions were: span/chord – 0.75 (stators) and 2.0 (rotors), pitch/chord – 0.75 (stators and rotors), span/diameter – 0.08. The stage group operates at the pressure drop from 88 to 70 bar, inlet temperature – 760 K, flow rate – 170 kg/s, average stage reaction – 0.15. It was assumed that the mass flow rate of the tip leakage over shrouded rotor blades amounted to 3% of the main stream flow rate. The hub leakage was neglected here. Tip leakage flow computations were then compared with those for leakage slots closed.

While leaving the main flow region, leakage flows (both at the tip and hub) help to remove the boundary layer fluid from the blade-to-blade passage upstream the rotor into the leakage slot, which retards the development of secondary flows. This effect can be observed from the comparison of velocity vectors at the blade suction surface of the first rotor for the two investigated variants of flow presented in Fig. 27. Sucking out the high-entropy boundary-layer fluid into the sink slot prior to the rotor brings a considerable reduction in the span-wise extension of the secondary flow zone and reduction of secondary flow losses as compared to non-source/sink computations.

Interesting is the development of secondary flows in the second stator. In Fig. 28, velocity vectors are shown in different blade-to-blade sections along the span of the second stator. In the tip leakage region, the incidence at the blade moves onto the suction surface where the stagnation point is situated. Besides the typical cross-flow from the pressure to the suction surface intensified by the non-nominal incidence, a reverse cross-flow from the suction surface is also observed at the front part of the blade, pushing the suction side leg of

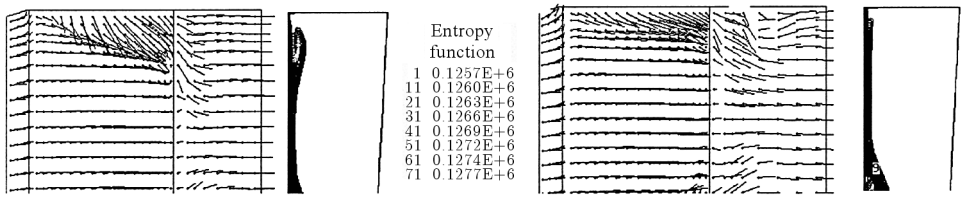

Fig. 27. Velocity vectors in the rotor (upper part) at the suction surface and entropy function contours at the rotor trailing edge – computed without sources and sinks (left), computed with tip leakage (right)

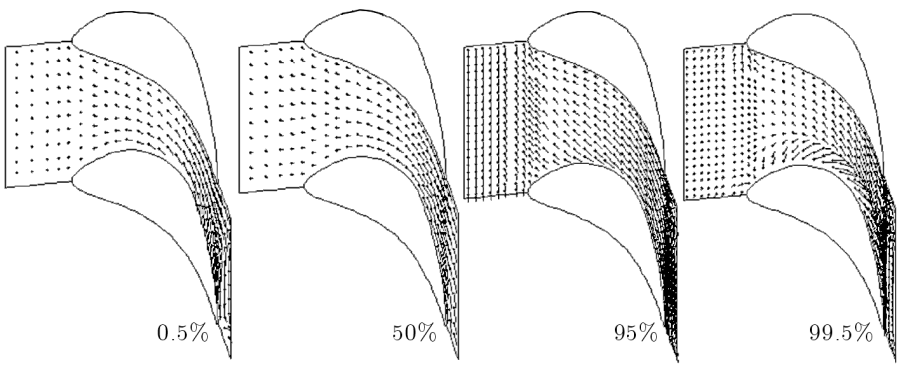

Fig. 28. Velocity vectors in the second stator at the hub 0.5% blade height from the hub, at the mid-span and in the tip leakage region 5% and 0.5% blade height from the tip

the horse-shoe vortex away from the suction surface. Due to the relocation of the stagnation point in the tip leakage region, another important factor that defines the flow patterns are strong span-wise pressure gradients at the blade surfaces in the tip endwall region. Static pressure contours and velocity vectors at the suction surface of the second stator blade are illustrated in Fig. 29. The downward pressure gradient at the suction surface in the front part of the passage induces motion of fluid elements in this direction. The opposite pressure gradient towards the tip endwall can be found at the pressure surface, giving rise to a strong recirculating flow, being a source of a large passage vortex that can be observed in the picture of secondary flow vectors in subsequent sections of the second stator, Fig. 30. This recirculating flow induced by local pressure gradients is much more intensive than that at the hub endwall and contains not only the boundary layer fluid but also the tip leakage fluid. Thus, the high-energy mixing zone of tip leakage flow is rolled up together with the endwall boundary layer into a strong structure of the passage vortex. Downstream, the centre of the passage vortex moves towards

the mid-span sections. In front part of the blade-to-blade passage, a thin layer of blocked reverse cross-flow is observed in the endwall/suction surface corner, being a source of vorticity of the sense of rotation opposite to that of the passage vortex.

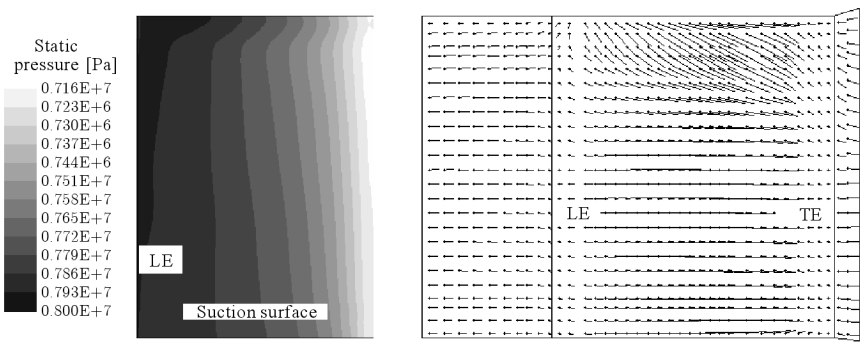

Fig. 29. Static pressure contours and velocity vectors at the suction surface of the second stator blade; LE – leading edge, TE – trailing edge

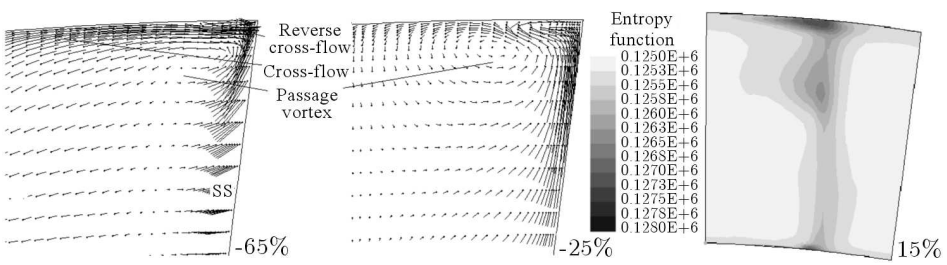

Fig. 30. Secondary flow vectors 35% and 75% axial chord downstream of the leading edge (left) and entropy function contours 15% axial chord downstream of the trailing edge in the second stator (right)

It is shown in Lampart (2006) that the total pressure surplus in the leakage-dominated region is gradually decreased along the second stator passage. Although the highest total pressure in the exit section is still observed in the upper part of the channel, most of the total pressure surplus is lost in the second stator. The loss centre due to the tip leakage from the upstream rotor moves together with the recirculating flow towards the suction surface and deep towards mid-span sections, Fig. 29. It is worthwhile to note that the increase in size and intensity of the tip passage vortex in the next stator due to the influence of the tip leakage flow was also observed in the experimental works of Peters *et al.* (2000) and Gibboni *et al.* (2003).

7. Other circumstances

Among other circumstances that have an effect on the development of secondary flows one can mention the *thickness and skewness of the inlet boundary layer* as well as *unsteady transport of 2D and 3D wakes* through downstream located cascades. These factors will not be discussed in detail in this paper but a reference will be made to publications, in which they are extensively described.

The thickness and skewness of the inlet boundary layer considerably affect both the development of secondary flows and the level of secondary flow losses in turbine cascades. It is shown in the experimental work of Gregory-Smith *et al.* (1988) that an increase in thickness of the boundary layer leads to an increase of extreme values in the distribution of vorticity and total pressure loss in the secondary flow regions, basically without a spacial displacement of these extremes. A double growth of the thickness of the inlet boundary layer is pronounced in a 50% increase of endwall losses.

The skewness of the boundary layer was experimentally investigated by Walsh and Gregory-Smith (1990). The situation applies when a straight (collateral) boundary layer passes from a stationary to a moving reference frame. The skewness can easily be explained with the help of a velocity triangle. Assuming that the main flow incidence is nominal, the low-velocity boundary layer fluid has an incidence moved onto the suction side, which coincides with the direcion of the endwall crossflow. Therefore, the skewness of the boundary layer intensifies the secondary flows. This situation refers to turbine flows and the reverse situation is typical for compressor flows. The skewness of the boundary layer in turbines leads to an increase in size of the passage vortex and its displacement towards the mid-span. The endwall losses may by increased by as much as 2/3 as compared to the no-skew situation.

The transport of stator wakes through the separation zone and secondary flow zone of the subsequent rotor cascade was investigated by Lampart (2006a). The transport of stator wakes was regarded as a passage of two-dimensional wakes skewed span-wise due to different convection velocities at the tip and hub, with a negligible effect of stator secondary flows. According to the velocity triangle, the passing wakes were found to periodically move the incidence at the rotor blade towards the suction side and reduce the flow turning in the cascade, which in turn leads to a periodic reduction of the intensity of the passage vortices and extension of the suction side separation.

Still, more complex is the transport of wakes from an unshrouded turbine rotor through the downstream stator cascade. The rotor wakes have a clearly

three-dimensional structure in the upper part of the channel dominated by the tip leakage vortex. The situation resembles to some extent the case of shrouded blading described in Section 6, however shows a pulsating nature due to periodically oncoming segments of the wake and tip vortex. The problem was investigated by Lampart (2006a,b), showing the presence of a pulsating recirculating flow in the second stator that encompasses the tip endwall boundary layer and segments of the co-rotating tip leakage vortex. The situation leads to formation of a large pulsating passage vortex.

8. Conclusions

The effects of main geometrical parameters and flow circumstances on the development of endwall flows and losses were investigated using the 3D RANS solver, including the effects of relative blade height, flow turning in the cascade, incidence angle, radial distribution of pressure and profile load as well as the effects of leakage flows and periodical wakes. A decrease of the relative blade height and/or increase of flow turning in the cascades and moving the incidence onto the pressure surface increases the intensity of passage vortices and the level of secondary flow losses. It was confirmed that for low blade heights and a high flow turning in the cascade, the secondary flow zones originating from the opposite endwalls merge at the mid-span section. Spanwise gradients of the pressure and profile load cause a redistribution of secondary loss centres along the blade span and endwall boundary layer losses.

The development of secondary flows for the case of non-nominal incidence angles onto the suction surface of the blade looks different than that described in textbooks for the classical case of nominal incidence. In this case, in the front part of the blade, the role of the convex and concave surface is reversed. The return to the typical turbine situation takes place in the rear part of the flow channel. As a result, two passage vortices can appear originating from specifically shaped endwall crossflows – a reverse (counter-rotating) passage vortex and a regular passage vortex.

Main properties of the interaction of the shroud leakage with the secondary flows were presented. The shroud leakage helps to remove the low-energy endwall boundary layer into the leakage slots, which retards the development of secondary flows in the current blade row. The inflow of the leakage stream onto the suction side of the downstream stator and local span-wise pressure gradients at the downstream stator blades induce a strong recirculating flow in the stator. This recirculating flow rolls up both the low-energy endwall boun-

dary layer fluid and a high-energy mixing layer of the shroud leakage and gives a rise to the formation of an intensive tip passage vortex in the stator. A large part of the total pressure surplus in the shroud leakage region is dissipated in the downstream stator.

It was also indicated that the transport of a two-dimensional stator wake leads to significant oscillations in the size of secondary flow zones, which can be explained by local changes of the inlet angle during the time of interaction with the passing wakes. Segments of the tip leakage vortex from unshrouded rotors are periodically found within the recirculating flow in the downstream stator, from which a strong pulsating passage vortex is formed.

References

1. Dejch M.,E., Filippov G.A., Lazarev L.Ja., 1965, *Collection of Profiles for Axial Turbine Cascades*, Machinostroienie, Moscow [in Russian]
2. Denton J.D., Xu L., 1999, The exploitation of 3D flow in turbomachinery design, *VKI LS*, 1999-02
3. Gardzilewicz A., Lampart P., Świrydczuk J., Kosowski K., 2000, Investigation of flow losses in turbine blading systems using CFD, Part I. Calculation method, *Turbomachinery (Cieplne Maszyny Przepływowe)*, **117**, 1, 179-186
4. Gibboni A., Menter J.R., Peters P., Wolter K., Pfost H., Breisig V., 2003, Interaction of labyrinth seal leakage flow and main flow in an axial turbine, *ASME Pap.*, GT2003-38722
5. Gregory-Smith D., Graves C.P., Walsh J.A., 1988, Growth of secondary losses and vorticity in an axial turbine cascade, *Trans. ASME J. Turbomachinery*, **110**, 1-8
6. Lampart P., 2006a, Investigation of aerodynamics of turbine blading systems using CFD methods, *Zeszyty Naukowe IMP PAN*, 544/1503/2006 [in Polish]
7. Lampart P., 2006b, Tip leakage flows in turbines, *TASK Quart.*, **10**, 2, 135-175
8. Lampart P., 2009, Investigation of endwall flows and losses in axial turbines. Part I. Formation of endwall flows and losses, *Journal of Theoretical and Applied Mechanics*, **47**, 2, 321-342
9. Lampart P., Gardzilewicz A., 1999, Numerical study of 3D blading in HP impulse turbines, *Cieplne Maszyny Przepływowe*, **115**, 297-310
10. Lampart P., Yershov S., Rusanov A., Szymaniak M., 2004, Tip leakage/main flow interactions in multi-stage HP turbines with short-height blading, *ASME Pap.*. GT2004-53882

11. PETERS P., BREISIG V., GIBONI A., LERNER C., PFOST H., 2000, The influence of the clearance of shrou-ded rotor blades on the development of the flowfield and losses in the subsequent stator, *ASME Pap.*, 2000-GT-478

12. *PŁK stator profile tables*, Rep. Zamech, Elbląg, Poland [in Polish]

13. TRAUPEL W., 1977, *Thermische Turbomaschinen*, Band I, Springer-Verlag, Berlin

14. WALSH J.A., GREGORY-SMITH G.D., 1990, Inlet skew and the growth of secondary losses and vorticity in a turbine cascade, *Trans. ASME, J. Turbomachinery*, **112**, 633-642

15. YAMAMOTO A., MATSYUNUMA T., OUTA E., 2001, Three-dimensional flows and losses in an ultrahighly loaded turbine, *Rep. National Aerospace Lab.*, Tokyo, Japan

16. YERSHOV S., RUSANOV A., 1997, *The Application Package FlowER for the Calculation of 3D Viscous Flows Through Multi-Stage Machinery*, Certificate of Registration of Copyright, Ukrainian State Agency of Copyright and Related Rights, Kiev

17. YERSHOV S., RUSANOV A., GARDZILEWICZ A., LAMPART P., ŚWIRYDCZUK J., 1998, Numerical simulation of viscous compressible flows in axial turbomachinery, *TASK Quart.*, **2**, 2, 319-347

Badanie przepływów i strat brzegowych w turbinach osiowych. Część II. Wpływ parametrów geometrycznych i przepływowych palisady

Streszczenie

W pracy przedstawiono wyniki obliczeń numerycznych wpływu parametrów geometrycznych i przepływowych palisady turbinowej na rozwój przepływów brzegowych. Rozważano wpływ stosunku wysokość/cięciwa łopatki, odchylenia przepływu w palisadzie, kąta wlotowego oraz promieniowego rozkładu ciśnienia i obciążenia profilu. Pokazano także jak zmienia się obraz przepływów wtórnych w przypadku nienominalnego napływu na stronę ssącą łopatki oraz podczas oddziaływania przepływu głównego z przeciekiem nadbandażowym i periodycznymi śladami spływowymi. Obliczenia wykonano z pomocą programu FlowER, solwera modelu 3D RANS.

Manuscript received June 20, 2008; accepted for print February 19, 2009